Kinetic Study of the Reaction $Ca^+ + N_2O$ from 188 to 1207 K

John M. C. Plane,* Tomas Vondrak, and Sarah Broadley

School of Environmental Sciences, University of East Anglia, Norwich NR4 7TJ, U.K.

Biljana Cosic,† Alexandre Ermoline, and Arthur Fontijn*

High-Temperature Reaction-Kinetics Laboratory, The Isermann Department of Chemical and Biological Engineering, Rensselaer Polytechnic Institute, Troy, New York 12180-3590

Received: March 17, 2006; In Final Form: May 2, 2006

Ion−molecule reactions involving metallic species play a central role in the chemistry of planetary ionospheres and in many combustion processes. The kinetics of the $Ca^+ + N_2O \rightarrow CaO^+ + N_2$ reaction was studied by the pulsed multiphoton dissociation at 193 nm of organo-calcium vapor in the presence of N_2O, followed by time-resolved laser-induced fluorescence spectroscopy of Ca^+ at 393.37 nm ($4^2P_{3/2} \leftarrow 4^2S_{1/2}$). This yielded $k(188-1207\ K) = 5.45 \times 10^{-11}\ (T/300\ K)^{0.53} \exp(282\ K/T)\ cm^3\ molecule^{-1}\ s^{-1}$, with an estimated accuracy of ±13% (188−600 K) and ±27% (600−1207 K). The temperature dependence of this barrierless reaction, with a minimum in the rate coefficient between 400 and 600 K, appears to be explained by the role of N_2O vibrational excitation. This is examined using a classical trajectory treatment on a potential energy surface calculated at the B3LYP/6-311+g(2d,p) level of theory.

Introduction

The ion−molecule reactions of metallic species are of interest over a very broad range of temperatures because of their importance in planetary ionospheres[1,2] and many combustion processes.[3−6] The major source of metals in the earth's upper mesosphere and lower thermosphere is the ablation of the 50−100 tons of interplanetary dust that enters the atmosphere daily, giving rise to layers of metal atoms and ions that extend globally between 80 and 120 km.[1] In the case of calcium, the layers of Ca and Ca^+ are observed using the ground-based lidar (laser radar) technique operating at 423.67 and 393.37 nm, respectively.[7]

Lidar observations have also revealed the phenomenon of sporadic Ca layers (Ca_s).[8] These are thin, concentrated layers of atomic Ca that occur at altitudes between 90 and 110 km, often appearing explosively within a few minutes. One theory for the formation of sporadic metal layers is the neutralization of the metallic ions in sporadic-*E* layers.[9] In the case of Ca^+, neutralization by radiative recombination ($Ca^+ + e^- \rightarrow Ca + h\nu$) is very slow.[10] Instead, conversion to Ca is likely to occur above 90 km by reaction with O_3 to form CaO^+, followed by dissociative recombination with an electron ($CaO^+ + e^- \rightarrow Ca + O$). Hence, one reason for studying the reaction

$$Ca^+ + N_2O \rightarrow CaO^+ + N_2 \qquad (1)$$

is as a convenient method for producing CaO^+ in the laboratory for further kinetic investigation.

Few direct kinetic measurements on ion−molecule reactions at combustion temperatures have been reported. Most work on such reactions has been done near or below room temperature. For higher temperatures, rate coefficients have mostly been estimated from reaction excitation functions measured with the molecular beam-gas technique; in this case effective temperatures, often different from kinetic (Boltzmann) temperatures, are calculated.[11] One exception in the past decade has been the work of Viggiano's group which developed a high-temperature (up to around 1800 K) flowing afterglow apparatus.[12] Among other achievements, they demonstrated the difference between rate coefficients obtained with this thermostated reactor and those from ion-drift tube measurements, where internal degrees of freedom are not equilibrated.[13] Their work has not included reactions of metallic species.

Metals are present in nearly all practical combustion systems as impurities or as inherent parts of the fuel, as e.g. in coal and municipal and industrial wastes.[3] Metals are also used as additives to modify burn and emission characteristics[4,5] and as major fuel components, such as in solid rocket propellants.[6] Most combustion systems are at least weakly ionized. The ions are in part due to thermal ionization of metal atoms which have low ionization potentials. Additionally, in the burning of fossil fuels and other organic compounds chemi-ions are produced by the well-known Calcote reaction $CH + O \rightarrow CHO^+ + e^-$. The CHO^+ ions in turn give rise to a wide variety of organic ions and H_3O^+.[14,15] These species usually have higher ionization potentials than metal atoms, such as the alkalis and the alkaline earths, to which their charges are transferred. As a result, even when the metals are present in small concentrations they can become the major positive charge carriers.[16]

Atomic ions can have a relatively long lifetime, as they would become neutralized by relatively slow radiative recombination or three-body recombination ($Ca^+ + e^- + M$, M = third body). Just as in the upper atmosphere, if such ions react to become molecular ions, then the much faster dissociative recombination route becomes available. Thus, the study of the oxidation of atomic metal ions, such as reported here, is important for determining the lifetimes or concentrations of charge carriers.

* Corresponding authors. J.M.C.P. e-mail: j.plane@uea.ac.uk. A.F. e-mail: fontia@rpi.edu.

† Present address: Department of Chemistry, University of Waterloo, Waterloo, Ontario, Canada.

10.1021/jp061664j CCC: $33.50
Published on Web 06/07/2006

A large and growing number of practical applications are based on the presence of ions and free electrons in flames.[15,17,18]

The pulsed laser photolysis−laser induced fluorescence (PLP-LIF) technique for studying metal ion reactions at low temperatures was pioneered by the group at the University of East Anglia (UEA).[19,20] Previously the Rensselaer Polytechnic Institute (RPI) group has studied a large number of reactions of metal−atoms, −monoxides, and −monohalides in the 300 to 1800 K temperature domain. Most of this work was done using HTFFR (high-temperature fast-flow reactor) facilities.[21,22] In some cases the HTP (high-temperature photochemistry−a specialized form of PLP-LIF) technique was also used,[23,24] and good agreement with HTFFR data[25] was obtained. The HTP technique is now adapted to the study of metal−ion reactions.

In the present paper we combine PLP-LIF measurements of the rate coefficients for reaction 1 (k_1) at low temperatures (188−371 K) from UEA with HTP data (470−1207 K) from RPI. In fact, the kinetics of reaction 1 at 300 K was first studied more than 30 years ago using the flowing−afterglow technique, which yielded $k_1 = (5.0^{+5.0}_{-2.5}) \times 10^{-11}$ cm^3 molecule^{-1} s^{-1}.[26] This is significantly smaller than a recent measurement of $(1.6 \pm 0.5) \times 10^{-10}$ cm^3 molecule^{-1} s^{-1} in an inductively coupled plasma/selected-ion flow tube apparatus with mass spectrometric detection,[27] and so a further measurement is desirable.

The temperature dependence of reaction 1 has not been studied previously. The reaction is exothermic ($\Delta H_0 = -169$ kJ mol^{-1}, see below), and exothermic ion−molecule reactions are expected to have very small temperature dependences−indeed, classical Langevin theory predicts that the rate coefficient should be independent of temperature.[28] However, it is interesting to note that the measured values of k_1 are less than 20% of the Langevin capture rate.[27] Furthermore, we have shown recently that the analogous reaction $Fe^+ + N_2O$ exhibits pronounced non-Arrhenius behavior: the rate coefficient has a positive temperature dependence above 300 K, but becomes essentially independent of temperature between 185 and 300 K.[29] We showed that this behavior could be explained by thermal excitation of the degenerate vibrational bending modes of N_2O, which overcomes the symmetry barrier associated with breaking the N_2-O bond to release the $O(^3P)$ atom. In the present paper we will examine this hypothesis in more detail−using ab initio quantum theory to explore the reaction potential energy surface, combined with trajectory calculations. Finally, the kinetic behavior of reaction 1 will be compared with the reactions

$$K + N_2O \rightarrow KO + N_2 \quad (2)$$

and

$$Ca + N_2O \rightarrow CaO + N_2 \quad (3)$$

which have both been studied previously over extended temperature ranges.[30−32] A comparison with reaction 2 is particularly interesting because K and Ca^+ are isoelectronic.

Experimental Section

UEA Experiments. The PLP-LIF apparatus at UEA has been described in detail previously.[19,31] Ca^+ ions were produced in the central chamber of the stainless steel reactor by the pulsed multiphoton photolysis of bis(2,2,6,6-tetramethyl-3,5-heptanedionato)calcium [$Ca(C_{11}H_{19}O_2)_2$, hereafter $Ca(TMHD)_2$] , in an excess of N_2O and bath gas (He). Powdered $Ca(TMHD)_2$ was placed in a tantalum boat located inside the heat pipe attached to the central chamber. The heat pipe temperature was then set in the range 389−417 K and maintained to within ±2 K during an experiment. The resulting $Ca(TMHD)_2$ vapor was entrained in a small flow of He bath gas and carried into the central chamber, where it mixed with larger flows of N_2O diluted in He. Photolysis of $Ca(TMHD)_2$ vapor at 193.3 nm, using a loosely focused ArF excimer laser (Lambda-Physik Compex 102, pulse energy ≈ 30 mJ, repetition rate 5 Hz), produced both Ca^+ and Ca.

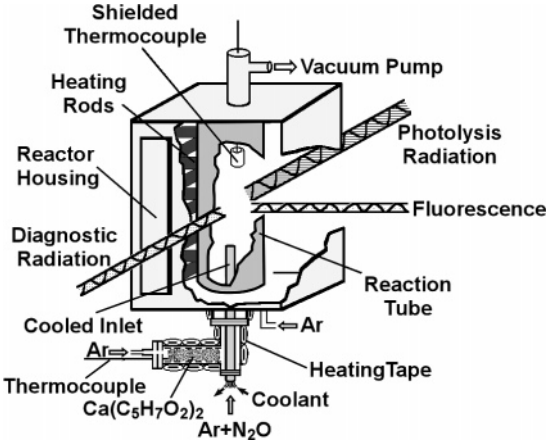

Figure 1. Diagram of the high-temperature photochemistry (HTP) reactor from RPI, used to study reaction 1 from 470 to 1207 K by the pulsed laser photolysis at 193 nm of Ca acetyl acetonate ($Ca(C_5H_7O_2)_2$) to produce Ca^+ in an excess of N_2O. The Ca^+ ions were probed by LIF at 393.37 nm.

Ca^+ was probed at 393.37 nm ($4^2P_{3/2} \leftarrow 4^2S$, $\tau = 6.8$ ns[33]) using a frequency-tripled Nd:YAG pumped dye laser (Sirah Model CBR-G-30, dye = 1:1 mixture of Exalite 389/Exalite 398; pulse energy = 10 μJ; bandwidth = 2×10^{-3} nm). The excimer and dye laser beams were collinear and counter-propagating, with the dye laser protected from the excimer beam by a dichroic reflector. The resonant LIF signal was detected orthogonal to the laser beams using a photomultiplier tube (Electron Tubes, 9816QB) after passing though an interference filter at 390 nm (fwhm = 10 nm), and then it was collected by a gated integrator (Stanford Research Systems, SR250) with a 30 ns wide gate triggered by the dye laser pulse. The dye laser was triggered at a scanned time delay after the excimer pulse, controlled by a microcomputer.

The reactor was enclosed in an electrically heated furnace, which could alternatively be filled with dry ice to carry out low-temperature measurements. The reaction temperature was measured just below the photolysis zone using a shielded chromel/alumel thermocouple. The decomposition of the precursor on the reactor walls above 418 K constrained the maximum temperature. The gases He (99.9999%, BOC Gases) and N_2O (99.9%, Air Products) were used without further purification. $Ca(TMHD)_2$ (99%, Strem Chemicals) was heated gently (∼370 K) under vacuum for about 1 h before use.

RPI Experiments. The basic HTP reactor design was similar to that used previously for neutral metal atom studies,[23−25] but with some important modifications that are illustrated in Figure 1. The reactor consists of a vertical alumina reaction tube, surrounded by four series of SiC resistance heating elements and insulating material, all enclosed in a water-cooled stainless steel vacuum housing. The reactor has four optical ports, at 90° separation and equipped with Suprasil quartz windows, which define the reaction zone. Ca^+ ions were produced by multiphoton photolysis of calcium acetyl acetonate [$Ca(C_5H_7O_2)_2$, hereafter CaAcAc]. The use of such a thermally unstable precursor, in combination with the high reaction temperatures,

required the vaporizer to be placed outside the high-temperature reactor (Figure 1). CaAcAc powder was therefore placed on a quartz boat in a side tube, which was heated independently by heating tape. Temperatures between 435 and 480 K were typically needed to initiate evaporation and/or thermal decomposition of the compound, which was entrained in a small flow of Ar (5−8% of the total gas flow rate).

When working at temperatures above 1000 K, an N_2O/Ar mixture was admitted into the reactor through a water-cooled movable inlet. This inlet was required to minimize the thermal dissociation of N_2O. The residence times between this inlet and the photolysis zone were selected so that mixing was at least 99% complete.[34,35] For most experiments at lower temperatures, N_2O was introduced with the main bath gas Ar flow through the bottom (upstream) plate of the reactor. The linear gas velocities were large enough to provide each photolysis pulse with a fresh reaction mixture. The temperature of the reaction zone was measured before and after each experiment with a Pt−Pt/13% Rh thermocouple, which for higher temperatures was shielded to minimize radiation effects.

CaAcAc was photolyzed by focusing 193 nm radiation from an ArF excimer laser (Lambda Physik Compex 201, operated at 1 Hz) with a 25 cm focal length plano-convex quartz lens. The 393.37 nm radiation from a XeCl excimer/dye laser combination (Lambda Physik LPX 100/FL3002, dye = 0.4 g L^{-1} PBBO in dioxane) was used to probe the Ca^+ resonance line. The resulting LIF signal passed through an interference filter at 396 nm (fwhm = 12 nm) and was detected by a PMT (EMI, model 9831 QA), equipped with a preamplifier (Stanford Research, SR 445A). The LIF signal was recorded at variable time delays between the photolysis and probe lasers using the same boxcar system as at UEA. The gases used were Ar (99.998%) from the liquid (Praxair) and 2% mixtures of N_2O in Ar prepared in the laboratory using N_2O (99.99%, Matheson). CaAcAc (99%, Alfa Aesar) was dried in the reactor, under vacuum, at 380 to 400 K for several hours before use.

Results

The experiments were carried out under pseudo-first-order conditions, where $[Ca^+] \ll [N_2O] \ll [\text{He or Ar}]$. The loss of Ca^+ can be described by a pseudo first-order decay coefficient, k', which can be written as

$$k' = k_{\text{diff, Ca}^+} + k_{\text{CaX}}[\text{CaX}] + k_1[N_2O] \qquad \text{(I)}$$

where the term $k_{\text{diff, Ca}^+}$ describes the diffusion of the Ca^+ atoms out of the volume defined by the intersection of the laser beams and within the field of view of the photomultiplier; k_{CaX} is the rate coefficient for reaction between Ca^+ and either the organometallic precursor (CaX) or degradation product(s), and the third term describes the loss of Ca^+ by reaction 1. Note that we are assuming here that the reaction between Ca^+ and N_2O only proceeds via the abstraction channel to form CaO^+ (reaction 1). This assumption is discussed below. As shown in Figure 2a, the observed decays of the LIF signal at low temperatures, with $Ca(TMHD)_2$ as the precursor, were well fitted by a single exponential from which k' was obtained. With CaAcAc as the precursor, the time-resolved LIF showed early growth to a maximum, followed by a region of nonexponential decay, and then, after a time t_i, by single-exponential decay. An example of this behavior is shown in Figure 2b. The initial growth of Ca^+ appears to be due to Ca^+ formation processes which persist for several microseconds after the pulsed photolysis of the precursor. t_i was found to vary between 10 and 200 μs range, depending upon reaction conditions. k' was obtained from these decays by fitting the LIF signal after t_i using a nonlinear least-squares fitting routine,[36] following a residual analysis and goodness-of-fit test[24,37] to confirm the single exponential form of the decay and determine t_i.

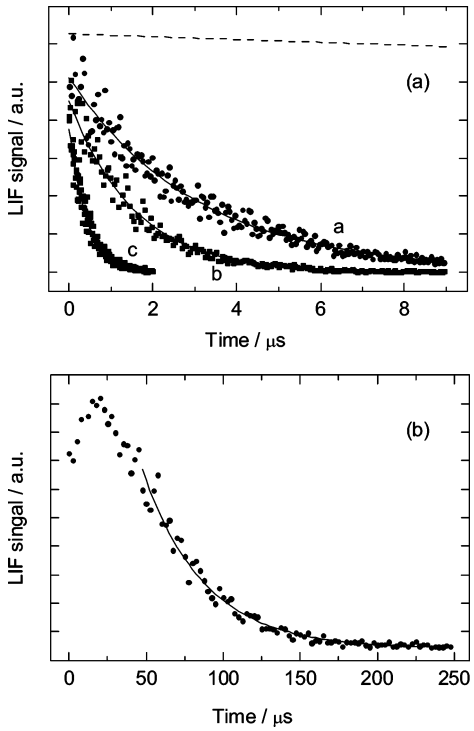

Figure 2. Examples of time-resolved Ca^+ LIF decays (solid points) and single-exponential fits (solid lines). (a) $T = 304$ K. $P = 20$ Torr. $[N_2O]$: a, 2.09×10^{15}; b, 4.20×10^{15}; c, 1.72×10^{16} molecule cm^{-3}. The dashed line indicates an LIF decay in the absence of N_2O. (b). $T = 661$ K. $P = 103.5$ Torr, $[N_2O] = 1.59 \times 10^{14}$ molecule cm^{-3}.

Figure 3a shows that the yield of Ca^+ from photolysis of $Ca(TMHD)_2$ depends on the square of the 193 nm excimer laser fluence, indicating that production of Ca^+ is probably a two-photon process. Two 193 nm photons provide a total of 12.9 eV, which is substantially more than the ionization potential of Ca (6.1 eV), so that 6.8 eV would in principle be available to dissociate the precursor. In the UEA experiments, the typical measured excimer fluence in the center of the chamber was 1.7×10^{17} photon cm^{-2}, so that ~1.5% of N_2O would have been photolyzed. This loss of N_2O in the reaction region was corrected for in the kinetic analysis. In the RPI work, rather higher excimer laser fluences were employed, and it was observed that k' (and hence k_1) decreased somewhat with increasing laser energy, as shown in Figure 3b. The $[N_2O] = 0$ data in this figure show no dependence on laser energy; furthermore, such an effect was not observed when O_2 was used[38] as a reactant rather than N_2O. This indicates that a small fraction of N_2O was dissociated under the multiphoton photolysis conditions used. To correct for this effect, the k' vs laser energy plots were all extrapolated to the intercepts on the ordinate (laser energy = 0) and the resulting values were used to obtain k_1.

When the dependence of k' on $[N_2O]$ was studied, the total pressure and flow rate of precursor was kept constant so that $k_{\text{diff, Ca}^+} + k_{\text{CaX}}[\text{CaX}]$ in equation I comprised the intercept of a plot of k' against $[N_2O]$. Plots of k' vs $[N_2O]$ at different temperatures are illustrated in Figure 4. Note that $[N_2O]$ was varied by at least a factor of 5 at each temperature. The slopes of the linear regression fits to these data sets yield k_1 (standard

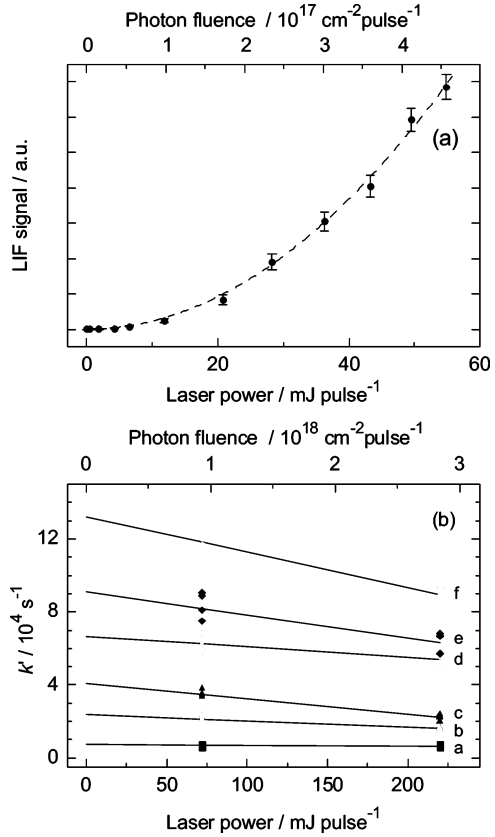

Figure 3. (a) Dependence of the Ca^+ LIF signal at 393.4 nm on the excimer (193 nm) laser power. The dashed line is a least-squares fit to a quadratic power law. The dye laser was triggered 80 μs after the excimer pulse, $P = 20$ Torr, $T = 308$ K. (b). Plots of k' vs 193 nm laser energy: $T = 898$ K. $P = 144.8$ Torr. [N_2O]: a, 0.00; b, 0.79×10^{14}; c, 1.64×10^{14}; d, 3.35×10^{14}; e, 5.07×10^{14}; f, 6.79×10^{14} molecule cm^{-3}.

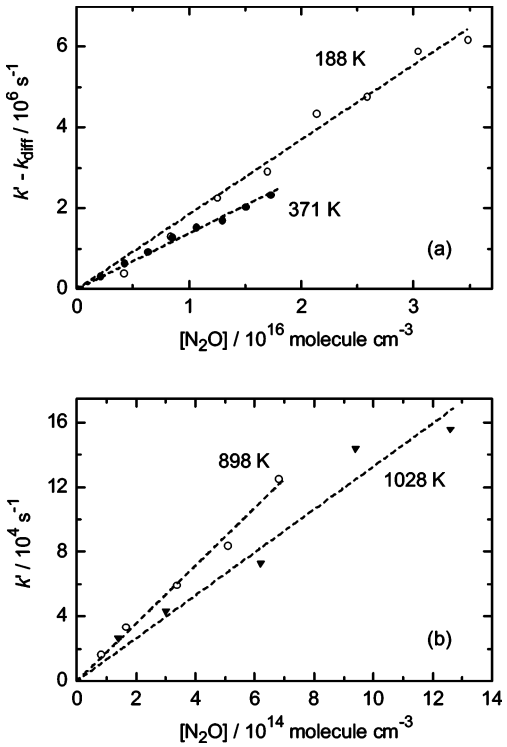

Figure 4. Plots of k' vs [N_2O]. Upper panel: $P = 20$ Torr. Lower panel: $P = 144.8$ Torr, obtained from k' extrapolated to zero 193 nm laser energy. The dashed lines are linear regression fits.

TABLE 1: Rate Coefficient $k_1(Ca^+ + N_2O)$ as a Function of Temperature

T/K	$(k_1 \pm \sigma_1)$/ 10^{-10} cm^3 $molecule^{-1}$ s^{-1}
188	1.89 ± 0.06
193	1.99 ± 0.07
209	1.73 ± 0.05
230	1.72 ± 0.05
249	1.53 ± 0.04
278	1.36 ± 0.05
304	1.43 ± 0.02
305	1.43 ± 0.03
306	1.43 ± 0.01
341	1.36 ± 0.05
359	1.37 ± 0.03
371	1.34 ± 0.03
478	1.26 ± 0.09
483	1.33 ± 0.11
563	1.28 ± 0.14
587	1.56 ± 0.08
613	1.36 ± 0.12
658	1.13 ± 0.14
661	1.05 ± 0.09
693	1.12 ± 0.18
730	0.98 ± 0.31
755	1.59 ± 0.11
755	1.22 ± 0.13
775	1.26 ± 0.05
790	1.28 ± 0.10
842	1.31 ± 0.11
898	1.79 ± 0.05
904	1.65 ± 0.18
932	1.58 ± 0.15
1028	1.33 ± 0.12
1133	1.63 ± 0.14
1207	1.09 ± 0.11

error σ_1) as a function of temperature, listed in Table 1. It was shown that k_1 is not pressure-dependent over the ranges 5−40 Torr (UEA) and 78−327 Torr (RPI). In the RPI experiments, k' was also shown to be independent of the gas velocity through the HTP reactor (when this was varied from 11 to 31 cm s^{-1}), as well as the distance of the CaAcAc/Ar sidearm or the cooled N_2O/Ar inlet from the photolysis zone.

Discussion

Figure 5 illustrates the temperature dependence of the rate coefficient for reaction 1. There is good agreement between the UEA and RPI results, extrapolating between 370 and 480 K. Although k_1 varies by less than a factor of 2 between 188 and 1207 K, the rate coefficient decreases between 188 and ∼550 K, and then increases slightly to 1207 K. A nonlinear regression fit to the data (see Figure 5) yields the following:

$$k_1(188-1207\ \mathrm{K}) = 5.45 \times 10^{-11}\,(T/300\ \mathrm{K})^{0.53} \exp(282\ \mathrm{K}/T)\ \mathrm{cm^3\ molecule^{-1}\ s^{-1}} \quad \text{(II)}$$

The resulting 2σ precision levels of the fit lie between ±4% (188−600 K) and ±15% (600−1207 K). Allowing ±12% and ±20% for systematic uncertainties in the lower and higher temperature ranges leads to overall accuracies of ±13% (188−600 K) and ±27% (600−1207 K) when using eq II to calculate k_1. It should be noted that this type of complex temperature dependence, where the rate coefficient decreases at low temperatures to a broad minimum before increasing again at high temperatures, has been observed previously in other ion−molecule reactions.[39,40]

Figure 5 also compares the results of the present study with two previous measurements of k_1 at room temperature. There

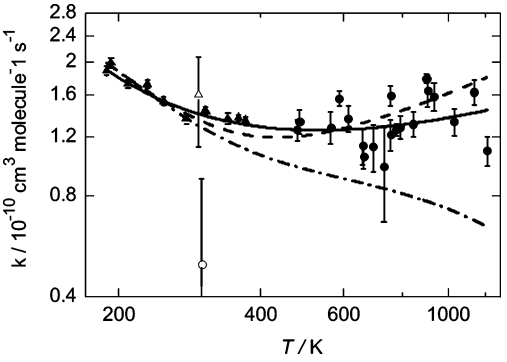

Figure 5. Temperature dependence of k_1: present study, UEA (filled triangles); present study, RPI (filled circles); Spears and Fehsenfeld[26] (open circle); Lavrov et al.[27] (open triangle); fit of eq II to the data from the present study (solid line); classical trajectory calculations including the effect of $N_2O(\nu_2)$ vibrational excitation (dashed line); trajectory calculations without $N_2O(\nu_2)$ excitation (dash−dot−dash line).

is good agreement, within experimental error, with the recent measurement by Lavrov et al.[27] using an inductively coupled plasma/selected-ion flow tube, which seems to confirm that the flowing afterglow measurements of Spears and Fehsenfeld[26] are too low by about a factor of 2.5.

Classical Langevin theory[28] predicts the capture rate between Ca^+ and N_2O to be $k_L = 8.9 \times 10^{-10}$ cm^3 molecule^{-1} s^{-1}, independent of temperature. When modified[41] to take account of the small permanent electric dipole of N_2O (0.161 D [42]), the capture rate varies from 9.4×10^{-10} cm^3 molecule^{-1} s^{-1} at 200 K to 9.1×10^{-10} cm^3 molecule^{-1} s^{-1} at 1200 K, about a factor of 6 times larger than the present measurements of k_1.

Potential Energy Surface for $Ca^+ + N_2O$. To understand why reaction 1 is relatively slow and has a complex temperature dependence, we used quantum calculations to examine the potential energy surface (PES) connecting $Ca^+ + N_2O$ to $CaO^+ + N_2$. The hybrid density functional/Hartree−Fock B3LYP method was employed from within the Gaussian03 suite of programs,[43] combined with the 6-311+G(2d,p) triple-ζ basis set. This is a large, flexible basis set which has both polarization and diffuse functions added to the atoms. At this level of theory, the expected uncertainty in the calculated cluster binding energies is ±14 kJ mol^{-1},[44] and the calculated bond lengths and (unscaled) vibrational frequencies of N_2O are within 0.9% and 3.6%, respectively, of the experimental quantities. The geometries, vibrational frequencies, rotational constants and relative energies of the relevant stationary points on the potential energy surfaces are listed in Table 2. Note that the calculated exothermicity of reaction 1 at 0 K is 169 kJ mol^{-1}.

The potential energy curves (corrected for zero-point energies) are illustrated in Figure 6. Figure 6a shows that for end-on attack of Ca^+ on the N_2O, a $Ca^+−N_2O$ complex forms initially (labeled Int 1). Note that this complex has a very low vibrational frequency (37 cm^{-1} — see Table 2), which corresponds to a bend of the Ca−O−N angle. The complex can then dissociate to $CaO^+ + N_2$ over a barrier of 24 kJ mol^{-1} (labeled TS 1), which is 30 kJ mol^{-1} below the reactant potential energy. However, reaching this transition state requires substantial rearrangement from Int 1 via a trans $Ca^+−O−N−N$ complex where the N_2O is bent: the Ca−O−N angle changes from 172° to 112°, and the O−N−N angle from 180° to 155°. Note that collinear attack of Ca^+ on N_2O is characterized by a large barrier associated with breaking the linear $O−N_2$ bond.

Figure 6b shows that for side-on attack, a more strongly bound cis complex forms where the N_2O wraps around the Ca^+ (labeled Int 2), before dissociating over a very low barrier to $CaO^+ + N_2$ (labeled TS 2). This is likely to be the route followed at low temperatures. Qualitatively, the small negative

TABLE 2: Geometries, Vibrational Frequencies, Rotational Constants, and Relative Energies of the Stationary Points on the PES for $Ca^+ + N_2O$ (Figure 6)

state designation	structure	vibrational frequencies[a]	rotational constants[b]	relative energy[c]
$Ca^+ + N_2O$	linear r(O−N) = 1.19Å r(N−N) = 1.12 Å	611 (×2), 1314, 2317	12.66	0
Int 1	planar r(Ca−O) = 2.35 Å r(O−N) = 1.21 Å r(N−N) = 1.11 Å −(Ca−O−N) = 172.4° −(O−N−N) = 179.0°	37, 196, 541, 541, 1279, 2376	1895, 1.732, 1.730	−54
TS 1	planar r(Ca−O) = 2.18 Å r(O−N) = 1.28 Å r(N−N) = 1.12 Å −(Ca−O−N) = 112.9° −(O−N−N) = 155.0°	513*i*, 94, 262, 463, 899, 2123	39.13, 2.421, 2.278	−30
Int 2	planar r(Ca−O) = 2.09 Å r(O−N) = 1.39 Å r(N−N) = 1.17 Å −(Ca−N−O) = 89.4° −(O−N−N) = 127.4°	241, 253, 426, 658, 679, 1766	13.22, 5.240, 3.753	−89
TS 2	planar r(Ca−O) = 2.04 Å r(O−N) = 1.55 Å r(N−N) = 1.14 Å −(Ca−O−N) = 90.4° −(O−N−N) = 124.4°	455*i*, 208, 236, 469, 607, 1904	12.75, 5.002, 3.592	−89
$CaO^+ + N_2$	r(Ca−O) = 1.99 Å	628	11.18	−169
$CaN^+(^3\Sigma) + NO$	r(Ca−N) = 2.15 Å	527	10.50	+318

[a] cm^{-1}. [b] GHz. [c] kJ mol^{-1}, with respect to $Ca^+(^2S) + N_2O$.

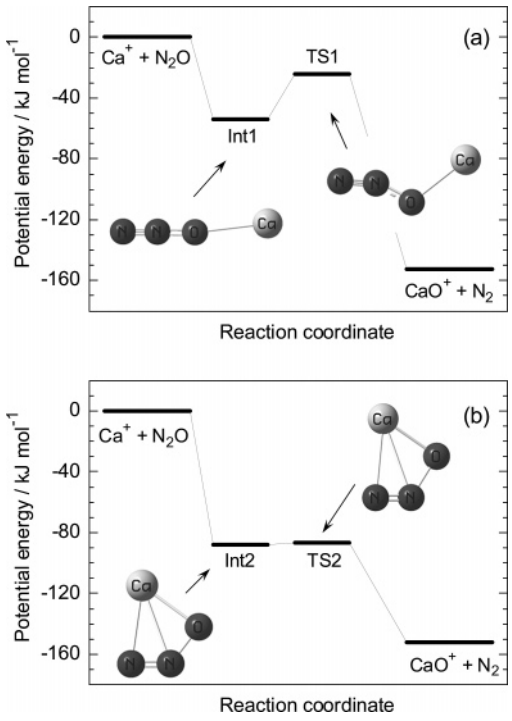

Figure 6. Potential energy curves for reaction 1, calculated at the B3LYP/6-311+g(2d,p) level of theory, for the cases of (a) end-on and (b) side-on attack of Ca^+ on N_2O.

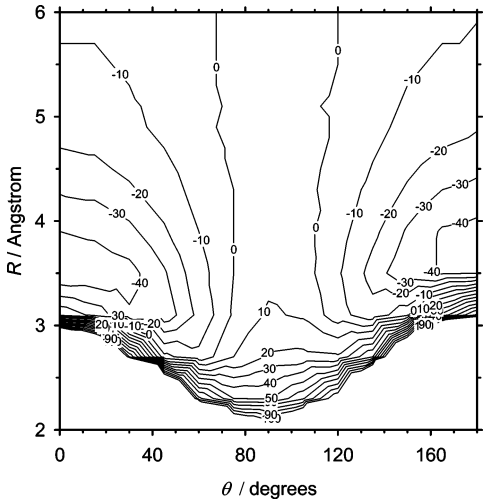

Figure 7. Potential energy surface for reaction 1 (kJ mol^{-1}) calculated at the B3LYP/6-311+g(2d,p) level of theory. The N_2O geometry is frozen. R and θ are defined in the text.

T dependence of k_1 is explained by the requirement that the Ca^+ must approach close to the central N of the N_2O in order to form the complex Int 2, before proceeding to products. At lower temperatures, collisions will have a higher probability of success because they will tend to occur with lower orbital angular momentum and also with less rotational excitation of the N_2O.

Figure 7 is a PES for the reaction, calculated with the geometry of N_2O frozen in order to study the longer-range interaction between the collision partners. The PES shows the potential energy as a function of the distance R between Ca^+ and X (the N_2O center-of-mass), and θ, the Ca^+-X-N_2 angle. Note that for near-collinear collision ($\theta \sim 0°$), there is a minimum on the PES at $R \sim 3.8$ Å, corresponding to Int 1 in Figure 6a. There is then a substantial barrier preventing the Ca^+ moving closer to the O atom in a nearly collinear geometry. Although there is a second minimum when θ is close to 180°, this does not lead to reaction. For the Ca^+ to approach closest to X, θ needs to be in the range 40°−80°.

Classical Trajectory Calculations. We now consider the collision dynamics between Ca^+ and N_2O in greater detail, by carrying out classical trajectory calculations using a treatment that we have applied previously to the reaction $Na^+ + N_2$.[45] We use an analytical form of the PES governing collisions between Ca^+ and N_2O in two dimensions, where the motion of the atoms is restricted to lie in a plane:[46]

$$V(R,\theta) = C[e^{-\varphi r_1} + e^{-\varphi r_2}] - \frac{\alpha(\theta)e^2}{2R^4} \qquad \text{(III)}$$

The distances r_1 and r_2 are from Ca^+ to O and from Ca^+ to the midpoint of the N−N bond, respectively; C and φ characterize the repulsive part of the interaction between Ca^+ and N_2O; and the anisotropic polarizability $\alpha(\theta)$ is given by

$$\alpha(\theta) = \frac{1}{2}(\alpha_p + \alpha_o) + \frac{1}{2}(\alpha_p - \alpha_o)\cos 2\theta \qquad \text{(IV)}$$

where α_p and α_o are the parallel and perpendicular polarizabilities of the N_2O molecule, respectively. The parameters α_p, α_o, C, and φ were optimized by a global fit of eq III to 274 points on the two-dimensional PES, which were calculated at the B3LYP/6-311+G(2d,p) level of theory. This procedure yielded the following: $\alpha_p = 1.54 \times 10^{-29}$ m^3, $\alpha_o = -2.3 \times 10^{-31}$ m^3, $C = 4.90 \times 10^{-17}$ J $molecule^{-1}$, and $\varphi = 2.77 \times 10^{10}$ m^{-1} (the small negative α_o arises from the best fit to the whole PES; it does not have physical significance).

Trajectories were then run on this surface using a classical Hamiltonian treatment.[45,47] The trajectories were initiated and terminated at $R = 20$ Å. To use this trajectory model to calculate k_1, we stipulated that a trajectory led to successful reaction if the Ca^+ ion approached within a critical distance of X, i.e. $R \leq R_c$. A set of trajectories was then run for a chosen temperature T. Values of the collision energy (E), impact parameter (b), rotational quantum number of N_2O (J), and θ were chosen using well-established pseudo-random techniques.[28,48] The integration was performed in the following sequence. First, a value of E was chosen, which then defines the Langevin impact parameter, b_{max}:[28]

$$b_{max} = \left(\frac{2\alpha_p e^2}{E}\right)^{1/4} \qquad \text{(V)}$$

Fifty trajectories were then run by selecting pseudo-randomly b, J, θ, and the direction of rotation of the N_2O rotor. Each trajectory was then tested to confirm that it met the orbiting criteria on the long-range potential, i.e. that $R < R^*$, where

$$R^* = \left(\frac{\alpha_p e^2}{Eb^2}\right)^{1/2} \qquad \text{(VI)}$$

The fraction $f(E)$ of reactive collisions is then given by the number of trajectories where $R < R_c$, to those where $R < R^*$. This sequence was then repeated at least 600 times by selecting further values of E pseudo-randomly, and the resulting $f(E)$ averaged to give $F(T)$. k_1 is then equal to $F(T) \cdot k_L$, and is thus computed from more than 3×10^4 individual trajectories.

Figure 8 shows histograms of the lifetimes of reactive trajectories at 200 and 1200 K, where the lifetime is defined as the time period between R^* and R_c. As expected, many trajectories last for over 10 ps, especially at 200 K. Indeed, the

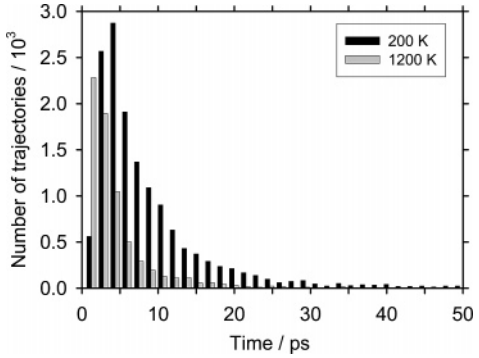

Figure 8. Histograms of reactive trajectory lifetimes for $Ca^+ + N_2O$ at 200 and 1200 K.

most likely trajectory lifetime at this temperature is 3−4 ps, and a few trajectories last for over 50 ps. Even at 1200 K, although the most likely lifetime is about 1 ps, some trajectories last for nearly 30 ps. These long lifetimes reflect the ability of the N_2O to orbit around the Ca^+ in the long-range $1/R^4$ potential. This is possible because there is very efficient transfer of orbital to rotational angular momentum in this system, since the N_2O behaves as a free rotor throughout most of its encounter with the Ca^+.

On the other hand, these trajectories do not last long enough for quenching by the He buffer gas to provide the possibility of stable $Ca^+ \cdot N_2O$ complex formation. For instance, at the highest pressures employed here (327 Torr by RPI), a lower limit to the quenching lifetime, given by the reciprocal of the product of the Langevin rate coefficient (for $Ca^+ \cdot N_2O$ + He) with [He], is ∼160 ps. This is considerably larger than the range of trajectory lifetimes in Figure 8.

The single adjustable parameter in this model is R_c. A very good fit to the low-temperature measurements of k_1 (dash−dot−dash line in Figure 5) is obtained with R_c = 2.9 Å. Inspection of Figure 8 shows that this condition is met when θ lies in the range ∼40°−80°, and this explains why k_1 is significantly lower than k_L. Note that although the model satisfactorily reproduces the negative temperature dependence of k_1 at temperatures below 400 K, it predicts that this dependence will continue at higher temperatures, in disagreement with the measurements (Figure 5).

As already discussed in the Introduction, several metal atom/ion + N_2O reactions exhibit non-Arrhenius behavior above 500 K, and this has been attributed to thermal excitation of the bending modes of N_2O enhancing the reaction cross section.[19,24,29,49] To examine the role of N_2O vibrational excitation in reaction 1, the trajectory model was extended to include the pseudo-random population of the degenerate bending modes of the N_2O. At the start of each trajectory, if the N_2O was selected to be vibrationally excited, then the reaction was deemed to occur if R approached closer than a second critical distance, R_c^{vib} (if the N_2O was not vibrationally excited, then the critical distance was R_c, as before). The trajectory model was then run to find the value of R_c^{vib} that produced a good fit to the experimental measurements of k_1 above 400 K. This was achieved with a value for R_c^{vib} of 3.2 Å, as shown in Figure 5 (dashed line). This result for R_c^{vib} indicates that a larger critical Ca^+−X separation is possible when the N_2O is vibrationally excited, because formation of both the cis and trans transition states (TS 2 and TS 1, respectively) are facilitated by the N_2O being bent.

We made the assumption earlier that the reaction between Ca^+ and N_2O only proceeds via abstraction to form CaO^+ (reaction 1). The reasoning behind this assumption is the following. First, the other possible abstraction channel is formation of CaN^+ + NO. However, quantum calculations (Table 2) show that formation of triplet CaN^+ is highly endothermic by 318 kJ mol^{-1}, and this channel will therefore not be significant even at the highest temperatures studied here. The reaction channel $Ca^+ \cdot NO$ + N is even less favorable, being endothermic by 342 kJ mol^{-1}. Second, complex formation via three-body recombination can be ruled out by the observed lack of a pressure dependence in k_1. Third, complex formation via two-body radiative recombination is a very ususual process, and would not be expected to be efficient when one of the reactants is closed-shell. Fourth, the mass spectrometric study of Lavrov et al.[27] has shown that CaO^+ is the only significant product.

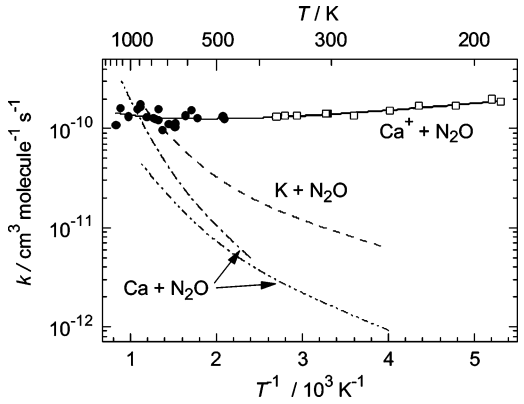

Figure 9. Arrhenius plots of the reactions $Ca^+ + N_2O$ (present study), K + N_2O (Plane[31]), and Ca + N_2O (Plane and Nien,[30] dash−dot−dot line; Vinckier et al.,[32] dash−dot−dash line).

Finally, it is interesting to compare the present measurements of reaction 1 with previous measurements of the analogous reactions of K[31] and Ca.[30,32] Figure 9 is an Arrhenius plot which shows that below 300 K, reactions 2 and 3 are, respectively, more than 1 and 2 orders of magnitude slower than reaction 1. Reaction 3 is the slowest reaction, presumably because Ca(4^1S) is a closed sub-shell species and therefore less reactive than K(4^2S) or Ca^+(4^2S). The difference between reaction 1 and 2 at low temperatures appears to be that while Ca^+ can form the relatively strongly bound complex with N_2O which leads to reaction (Figure 6b), this barrierless pathway is not available to the neutral K atom: quantum calculations show that it cannot form a complex analogous to Int 2. Since reactions 2 and 3 have larger activation energies than reaction 1, their rate coefficients approach k_1 at around 1000 K. Note that the activation energies of reactions 2 and 3 also increase above 500 K, which again is most likely caused by vibrational excitation of N_2O enhancing their reaction cross sections.

Conclusions

The use of the PLP-LIF technique in two different reactors has enabled the kinetic measurements for a metal-ion molecule reaction to span an unusually large temperature range. The domain covered spans temperatures of direct ionospheric interest and those of direct combustion interest. The combination of high temperatures with pressures above a few Torr has apparently not been achieved in prior ion−molecule reaction studies. The $Ca^+ + N_2O$ rate coefficients show a small, but complex, dependence on temperature, with a minimum between about 400 and 600 K. This behavior, which deviates from Langevin theory, is well explained by the present classical trajectory treatment.

Acknowledgment. The work at UEA was supported by NERC grant NE/B00015X/1, and that at RPI by NSF grant CTS − 0224778. We thank Dr. A. A. Viggiano for helpful discussions and W. F. Flaherty for assistance.

References and Notes

(1) Plane, J. M. C. *Chem. Rev.* **2003**, *103*, 4963.
(2) Patzold, M.; Tellman, S.; Hausler, B.; Hinson, D.; Schaa, R.; Tyler, G. L. *Science* **2005**, *310*, 837.
(3) Tillman, D. A. *Trace metals in Combustion Systems*; Academic Press: San Diego, 1994.
(4) Howard, J. B.; Kausch, W. J. *Prog. Energy Combust. Sci.* **1980**, *6*, 263.
(5) Rumminger, M. D.; Reinelt, D.; Babushok, V.; Linteris, G. T. *Combust. Flame* **1999**, *116*, 207.
(6) Sutton, G. P. *Rocket Propulsion Elements*, 5 ed.; John Wiley: New York, 1986.
(7) Gerding, M.; Alpers, M.; von Zahn, U.; Rollason, R. J.; Plane, J. M. C. *J. Geophys. Res-Space Phys.* **2000**, *105*, 27131.
(8) Alpers, M.; Hoffner, J.; vonZahn, U. *Geophys. Res. Lett.* **1996**, *23*, 567.
(9) Cox, R. M.; Plane, J. M. C. *J. Geophys. Res.-Atmos.* **1998**, *103*, 6349.
(10) Nahar, S. N.; Bautista, M. A.; Pradhan, A. K. *Astrophys. J.* **1997**, *479*, 497.
(11) Lindinger, W.; Smith, D. In *Reactions of Small Transient Species. Kinetics and Energetics*; Fontijn, A., Clyne, M. A. A., Eds.; Academic press: London, 1983.
(12) Hierl, P. M.; Friedman, J. F.; Miller, T. M.; Dotan, I.; MenendezBarreto, M.; Seeley, J. V.; Williamson, J. S.; Dale, F.; Mundis, P. L.; Morris, R. A.; Paulson, J. F.; Viggiano, A. A. *Rev. Sci. Instrum.* **1996**, *67*, 2142.
(13) Hierl, P. M.; Dotan, I.; Seeley, J. V.; VanDoren, J. M.; Morris, R. A.; Viggiano, A. A. *J. Chem. Phys.* **1997**, *106*, 3540.
(14) Calcote, H. F.; Kurzius, S.; Miller, W. J. *Proceedings of the Combustion Institute* **1965**, *10*, 605.
(15) Lawton, J.; Weinberg, F. J. *Electrical Aspects of Combustion*; Clarendon: Oxford, 1969.
(16) Sugden, T. M. *Sci. Prog.* **1963**, *51*, 177.
(17) *Advanced Combustion Methods*; Weinberg, F. J., Ed.; Academic Press: London, 1986.
(18) Weinberg, F. J. *Combust. Sci. Technol.* **1994**, *98*, 349.
(19) Plane, J. M. C.; Rollason, R. J. *J. Chem. Soc.-Faraday Trans.* **1996**, *92*, 4371.
(20) Rollason, R. J.; Plane, J. M. C. *J. Chem. Soc.-Faraday Trans.* **1998**, *94*, 3067.
(21) Fontijn, A.; Futerko, P. M. In *Gas-Phase Metal Reactions*; Fontijn, A., Ed.; North-Holland: Amsterdam, 1992.
(22) Fontijn, A. *Pure Appl. Chem.* **1998**, *70*, 469.
(23) Marshall, P.; Narayan, A. S.; Fontijn, A. *J. Phys. Chem.* **1990**, *94*, 2998.
(24) Narayan, A. S.; Futerko, P. M.; Fontijn, A. *J. Phys. Chem.* **1992**, *96*, 290.
(25) Fontijn, A.; Blue, A. S.; Narayan, A. S.; Bajaj, P. N. *Combust. Sci. Technol.* **1994**, *101*, 59.
(26) Spears, K. G.; Fehsenfeld, F. C. *J. Chem. Phys.* **1972**, *56*, 5698.
(27) Lavrov, V. V.; Blagojevic, V.; Koyanagi, G. K.; Orlova, G.; Bohme, D. K. *J. Phys. Chem. A* **2004**, *108*, 5610.
(28) Smith, I. W. M. *Kinetics and Dynamics of Elementary Gas Reactions*; Butterworth: London, 1980.
(29) Vondrak, T.; Woodcock, K. R. S.; Plane, J. M. C. *Phys. Chem. Chem. Phys.* **2006**, *4*, 503.
(30) Plane, J. M. C.; Nien, C. F. *J. Phys. Chem.* **1990**, *94*, 5255.
(31) Plane, J. M. C. A Comparison between the Oxidation Reactions of the Alkali and Alkaline Earth Atoms. In *Gas-Phase Metal Reactions*; Fontijn, A., Ed.; Elsevier: Amsterdam, 1992; p 29.
(32) Vinckier, C.; Helaers, J.; Remeysen, J. *J. Phys. Chem. A* **1999**, *103*, 5328.
(33) Radzig, A. A.; Smirnov, B. M. *Reference Data on Atoms, Molecules, and Ions*; Springer-Verlag: Berlin, 1985.
(34) Marshall, P.; Ko, T.; Fontijn, A. *J. Phys. Chem.* **1989**, *93*, 1922.
(35) Riley, P. S.; Cosic, B.; Fontijn, A. *Int. J. Chem. Kinet.* **2003**, *35*, 374.
(36) Marshall, P. *Comput. Chem.* **1987**, *11*, 219.
(37) Ko, T.; Adusei, G. Y.; Fontijn, A. *J. Phys. Chem.* **1991**, *95*, 8745.
(38) Cosic, B.; Ermoline, A.; Fontijn, A. Work in progress.
(39) Miller, T. M.; Friedman, J. F.; Williamson, J. S.; Viggiano, A. A. *J. Chem. Phys.* **2006**, *124*.
(40) Popovic, S.; Midey, A. J.; Williams, S.; Fernandez, A. I.; Viggiano, A. A.; Zhang, P.; Morokuma, K. *J. Chem. Phys.* **2004**, *121*, 9481.
(41) Troe, J. *J. Chem. Phys.* **1987**, *87*, 2773.
(42) Lide, D. R. *Handbook of Physics and Chemistry*; CRC Press: Boca Raton, FL, 1992; Vol. 72rd ed.
(43) Frisch, M. J.; Trucks, G. W.; Schlegel, H. B.; Scuseria, G. E.; Robb, M. A.; Cheeseman, J. R.; J. A. Montgomery, J.; Vreven, T.; Kudin, K. N.; Burant, J. C.; Millam, J. M.; Iyengar, S. S.; Tomasi, J.; Barone, V.; Mennucci, B.; Cossi, M.; Scalmani, G.; Rega, N.; Petersson, G. A.; Nakatsuji, H.; Hada, M.; Ehara, M.; Toyota, K.; Fukuda, R.; Hasegawa, J.; Ishida, M.; Nakajima, T.; Honda, Y.; Kitao, O.; Nakai, H.; Klene, M.; Li, X.; Knox, J. E.; Hratchian, H. P.; Cross, J. B.; Adamo, C.; Jaramillo, J.; Gomperts, R.; Stratmann, R. E.; Yazyev, O.; Austin, A. J.; Cammi, R.; Pomelli, C.; Ochterski, J. W.; Ayala, P. Y.; Morokuma, K.; Voth, G. A.; Salvador, P.; Dannenberg, J. J.; Zakrzewski, V. G.; Dapprich, S.; Daniels, A. D.; Strain, M. C.; Farkas, O.; Malick, D. K.; Rabuck, A. D.; Raghavachari, K.; Foresman, J. B.; Ortiz, J. V.; Cui, Q.; Baboul, A. G.; Clifford, S.; Cioslowski, J.; Stefanov, B. B.; Liu, G.; Liashenko, A.; Piskorz, P.; Komaromi, I.; Martin, R. L.; Fox, D. J.; Keith, T.; Al-Laham, M. A.; Peng, C. Y.; Nanayakkara, A.; Challacombe, M.; Gill, P. M. W.; Johnson, B.; Chen, W.; Wong, M. W.; Gonzalez, C.; Pople, J. A. *Gaussian 03, Revision B.03*; Gaussian Inc.: Pittsburgh, PA, 2003.
(44) Foresman, J. B.; Frisch, A. *Exploring chemistry with electronic structure methods*; Gaussian, Inc.: Pittsburgh, PA, 1996.
(45) Cox, R. M.; Plane, J. M. C. *J. Chem. Soc.-Faraday Trans.* **1997**, *93*, 2619.
(46) Ramachandran, G.; Ezra, G. S. *J. Phys. Chem.* **1995**, *99*, 2435.
(47) Schelling, F. J.; Castleman, A. W. *Chem. Phys. Lett.* **1984**, *111*, 47.
(48) Bunker, D. L. *Theories of Elementary Gas Reactions*; Pergamon: Oxford, 1966.
(49) Plane, J. M. C. *J. Phys. Chem.* **1987**, *91*, 6552.